Spatiotemporal profiles of arginine vasopressin transcription in cultured suprachiasmatic nucleus

Tomoko Yoshikawa[1,2], Yoshihiro Nakajima[3], Yoshiko Yamada[1,2], Ryosuke Enoki[1,2,4], Kazuto Watanabe[5], Maya Yamazaki[6], Kenji Sakimura[6], Sato Honma[2], Ken-ichi Honma[2]

[1]Photonic Bioimaging Section, [2]Department of Chronomedicine, Hokkaido University Graduate School of Medicine, Sapporo 060-8638, Japan, [3]Health Research Institute, National Institute of Advanced Industrial Science and Technology (AIST), Kagawa 761-0395, Japan, [4]Precursory Research for Embryonic Science and Technology (PRESTO), Japan Science and Technology Agency (JST), Saitama 332-0012, Japan, [5]Department of Regulatory Physiology, Dokkyo Medical University School of Medicine, Tochigi 321-0293, Japan, [6]Department of Cellular Neurobiology, Brain Research Institute, Niigata University, Niigata 951-8585, Japan

Corresponding author:
Dr. Ken-ichi Honma
Department of Chronomedicine, Hokkaido University Graduate School of Medicine, N15 W7, Kita-ku, Sapporo 060-8638, Japan
Tel +81-11-706-4777
Fax +81-11-706-4737
E-mail kenhonma@med.hokudai.ac.jp

Running title: Spatiotemporal profiles of AVP transcription in the SCN

Total number of pages 32
Total number of figures 6

Total number of words in:	(i) Whole manuscript	8818
	(ii) Abstract	243
	(iii) Introduction	484

Keywords: AVP-ELuc, bioluminescence, circadian rhythm, SCN, mouse

Abbreviations: a.u., arbitrary unit; AVP, arginine vasopressin; CT, circadian time; DD, constant dark; eGFP, enhanced green fluorescent protein; ELuc, Emerald-luciferase; hnRNA, heteronuclear RNA; LD, light: dark; OC, optic chiasm; PFA, paraformaldehyde; PMT, photomultiplier tube; PR, percent rhythm; PVN, paraventricular nucleus; RLU, relative light unit; ROI, region of interest; SCN, suprachiasmatic nucleus; SON, supraoptic nucleus; V, third ventricle; VIP, vasoactive intestinal peptide; WT, wild type; ZT, Zeitgeber time

There are no conflicts of interest to declare.

Abstract

Arginine vasopressin (AVP), a major neuropeptide in the suprachiasmatic nucleus (SCN), is postulated to mediate the output of the circadian oscillation. Mice carrying a reporter gene of AVP transcription (AVP^{ELuc}) were produced by knocking-in a cDNA of Emerald-luciferase (ELuc) in the translational initiation site. Homozygous mice did not survive beyond postnatal day 7. Using the heterozygous ($AVP^{ELuc/+}$) mice, we developed a bioluminescence reporter system that enabled us to monitor AVP transcription through AVP-ELuc measurement in real time for more than 10 cycles in the cultured brain slice. $AVP^{ELuc/+}$ mice showed circadian behavior rhythms and light responsiveness indistinguishable from those of the wild type. Robust circadian rhythms in AVP-ELuc were detected in the cultured SCN slice at a single cell as well as tissue levels. The circadian rhythm of the whole SCN slice was stable, with the peak at mid-light phase of a light-dark cycle, while that of a single cell was more variable. By comparison, rhythmicity in the paraventricular nucleus and supraoptic nucleus in the hypothalamus was unstable and damped rapidly. Spatiotemporal profiles of AVP expression at pixel level revealed significant circadian rhythms in the entire area of AVP positive cells in the SCN, and at least two clusters which showed different circadian oscillations. Contour analysis of bioluminescence intensity in a cell-like region demonstrated the radiation area was almost identical to the cell size. This newly developed reporter system for AVP gene expression is a useful tool for the study of circadian rhythms.

Introduction

Arginine vasopressin (AVP) is a major neuropeptide in the suprachiasmatic nucleus (SCN), location of the circadian pacemaker. Most SCN cells exhibit circadian rhythms in clock gene expression and electrical activity (Welsh *et al.*, 1995; Yamaguchi *et al.*, 2003). The cellular circadian rhythms are rather variable but integrated by oscillatory couplings to build up a coherent circadian rhythm on tissue level (Inagaki *et al.*, 2007). AVP neurons are distributed in the shell region, while neurons containing vasoactive intestinal peptide (VIP), another major neuropeptide in the SCN, distribute in the core region (Moore *et al.*, 2002). AVP and VIP exhibit robust circadian rhythms in production, storage, and secretion (Shinohara *et al.*, 1993; Ban *et al.*, 1997; Francl *et al.*, 2010; Kalsbeek *et al.*, 2010). However, we have observed that the circadian rhythms become desynchronized in SCN slice culture (Shinohara *et al.*, 1995), indicating that AVP and VIP neurons have independent circadian oscillators. There might be two classes of coupling: one synchronized among the AVP or VIP neurons and the other between the AVP and VIP circadian rhythms. Recently, the importance of AVP in intra-SCN oscillatory coupling has been recognized (Mieda *et al.*, 2015). Mice genetically deficient in AVP receptors re-entrained immediately to a phase-shift of the light-dark (LD) cycle (Yamaguchi *et al.*, 2013).

AVP-positive SCN neurons extend their axons to structures outside the SCN (Rood & De Vries, 2011). AVP was found in the cerebrospinal fluid and thought to originate from the SCN (Schwartz & Reppert, 1985). This AVP could be a mediator of SCN circadian signals to the extra-SCN areas. AVP-containing cells are also localized in the paraventricular nucleus (PVN) and supraoptic nucleus (SON) (Rood & De Vries, 2011). AVP in these nuclei are produced in the cell body and transported to the posterior

pituitary, where AVP is stored and released into the general circulation in response to various stimuli (Iovino *et al.*, 2012). Circadian dynamics of AVP in the SCN and other nuclei are not well documented. And there are inconsistencies regarding circadian phase in the literature (Noto *et al.*, 1983; Yamase *et al.*, 1991). One of the reasons for these ambiguities is the lack of analytical tools for monitoring the dynamics of AVP production and secretion with high temporal and spatial resolution. Recent advances in gene engineering and photonic bioimaging techniques have made it possible to monitor transcription of a gene of interest using a specific bioluminescent reporter (Millar *et al.*, 1992). Ueta *et al*., (2005) reported AVP gene expression in transgenic rats producing an AVP-eGFP fusion protein. However, it was difficult to monitor the eGFP fluorescence continuously over several days, an operation that is mandatory for biological rhythm studies.

Here we report a newly generated knock-in mouse carrying a luciferase reporter of AVP expression that allows monitoring AVP transcription in cultured brain slices containing the SCN, PVN or SON. A novel technology revealed robust circadian rhythms in AVP expression for many cycles.

Materials and methods

Animal experiments were conducted in accordance with the Guidelines for the Care and Use of Laboratory Animals of Hokkaido University and Niigata University. The present experiments were approved by the Animal Research Committee of Hokkaido University and Niigata University (permission numbers 130064 for Hokkaido University and 178-8 for Niigata University).

Generation of AVP^{ELuc} *knock-in mouse*

To generate the AVP^{ELuc} knock-in mouse, we designed a targeting vector in which the Emerald-luciferase gene (Nakajima *et al.*, 2010) (TOYOBO, Osaka, Japan) along with PEST, SV40, and polyA sequences (ELuc) were inserted into the translational initiation site of the mouse *AVP* gene in frame (Fig. 1A). The half-life of Eluc::PEST is 2.8 h (Yasunaga *et al.*, 2015). The knock-in vector was constructed with 11.67 kb C57BL/6 genomic fragment (5.3 kb upstream and 6.37 kb downstream from the translational initiation site), a neomycin resistance cassette, and a diphtheria toxin gene using BAC subcloning kit (Gene Bridges, Dresden, Germany). The linearized targeting vector was electroporated into the C57BL/6N embryonic stem cell line RENKA (Mishina & Sakimura, 2007). Correctly targeted clones were identified by Southern blotting using 5′, 3′, and neo probes (Fig. 1B). Chimeric mice were obtained as described previously (Fukaya *et al.*, 2006).

Genotypes were determined by PCR of mouse tail genomic DNA using the following primers: forward 5′-TCCTAGGGAACACCTGCAGACAT-3′, reverse for wild type (WT) 5′-CAGTATCCTTTATGCGGCTTCTCTAGCACC-3′, and for knock-in line 5′-AGATGTTCCTGTGGGTCTGC-3′. The PCR product sizes of the WT and knock-in mice were 410 bp and 712 bp, respectively (Fig. 1C). Heterozygous mice ($AVP^{ELuc/+}$) were used for further analysis.

Plasma AVP level was determined in $AVP^{ELuc/+}$ and C57BL/6 mice in the middle of the light phase and there was no significant difference between them ($AVP^{ELuc/+}$; 114.8 ± 28.7 pg/ml, n = 5; C57BL/6J, 127.1 ± 30.2 pg/ml, n = 5).

Animal housing

Wild type and AVP^{ELuc} knock-in mice were bred and raised in the animal facility at Hokkaido University under LD cycles with lights on at 06:00 h and off at 18:00 h. Light intensity during the light phase was approximately 100 lux. Room temperature was 22 ± 2°C and humidity was 60 ± 10%. The mice were fed commercial chow and tap water ad libitum. Experiments were performed under LD cycles unless otherwise specified. WT and $AVP^{ELuc/+}$ male mice were used *in vivo* experiments, and both sexes were used in *ex vivo* experiments.

Measurements of body weight, water, and food intake

$AVP^{ELuc/+}$ and littermate WT mice were used for the experiments. Because homozygotes did not survive more than 7 days, we used heterozygotes. Body weight of $AVP^{ELuc/+}$ (n = 12) and littermate WT (n = 13) was measured weekly from ages 1 to 10 weeks. Water and food intake were also measured together with body weight in $AVP^{ELuc/+}$ (n = 4) and WT (n = 5) mice from ages 6 to 12 weeks.

Measurement of spontaneous locomotor activity and data analyses

$AVP^{ELuc/+}$ (n = 10) and their littermate WT (n = 5) mice of 4 months old were transferred into individual cages in light-tight boxes where light intensity was approximately 300 lux in the light phase. Spontaneous locomotor activity was measured by a thermal sensor as described elsewhere (Nishide *et al.*, 2006). Mice were kept in LD for 22 days and released into constant dark (DD). A single light pulse of 30 min (300 lux) was given at circadian time (CT) 14 on day 19 and at CT22 on day 40 in DD, where the onset of an activity band in the behavior rhythm (activity onset) was

designated as CT12. Activity was recorded every min with a PC system (Stanford Chronokit, Stanford Software Systems, CA, USA) and analyzed with Clock Lab (Actimetrics, IL, USA). The free-running period was determined from an eye-fitted line, which was drawn through the onsets of the activity band in steady state free-run before application of the first light pulse. Magnitude of phase shifts by a light pulse was defined as a phase difference on the next day of a pulse between the activity onset of a pre-pulse free-running rhythm and the extrapolated regression line fitted to the activity onset in a post-pulse steady state free-run (steady-state phase shifts).

In situ hybridization

$AVP^{ELuc/+}$ (n=10) and littermate WT (n=10) mice were used for *in situ* hybridization. Brain samples were collected at Zeitgeber Time (ZT) 6 and 18, where the light onset of LD was designated as ZT 0. Coronal brain slices of 20 μm thick were subjected to the hybridization according to the protocol described previously (Baba *et al*, 2008). Antisense oligonucleotide complimentary to mouse AVP-Neurophysin II (457~504) (5'-GTAGACCCGGGGCTTGGCAGAATCCACGGACTCCCGTGTCCC AGCCAG-3') was labeled with ^{33}P dATP using terminal deoxyribonucleotidyl transferase (Gibco BRL). The brain slices were air dried and exposed to BioMax MR films (Eastman Kodak) for 2 days (from day 5 to day 7 after hybridization) with the ^{14}C acrylic standard (American Radiolabeled Chemicals). Autoradiography was analyzed with the image analysis system (MCID Core, MCID Image Analysis Software Solutions for Life Sciences), and the optical density was converted to the relative radioactive value (kBq / g) with the ^{14}C acrylic standard. The amount of mRNA per unit area in

each mouse was expressed as the mean of three consecutive slices in the calibrated OD (kBq / g).

Immunohistochemistry

The **distribution** of AVP neurons in the SCN of $AVP^{ELuc/+}$ mice was examined by semi-quantitative immunohistochemical analysis. The WT (n=4) and $AVP^{ELuc/+}$ mice (n = 4) were anesthetized with ether and transcardially perfused with saline followed by 4% paraformaldehyde (PFA). The brains were post-fixed with 4% PFA. The coronal slices of 20 μm thick including the SCN were prepared by a cryostat (Leica, Germany) and mounted on PLATIMUM-PRO coated glass slides (Matsunami, Osaka, Japan). For this analysis, slices containing the middle potion of the SCN were used. The slices were washed with Tris-buffered saline (TBS) and then blocked by 10% normal goat serum (NGS) dissolved in TBS containing 0.4% Triton X-100 at room temperature. The slices were incubated in a mixture of mouse anti-AVP antibody (AVP-NP, PS41) (Romijn *et al.*, 1997) and rabbit ant-VIP antiserum (Peptide Institute, Osaka, Japan) in TBS containing 2% NGS and 0.4% Triton X-100 (TTG) at 4°C. After washing with TTG, the slices were incubated with secondary antibodies labeled with Alexa (anti-mouse IgG, A11008 and anti-rabbit IgG, A11005, Invitrogen) in TTG at 4°C. The slices were washed with TBS and sealed with Prolong Gold with DAPI (Invitrogen). AVP and VIP signals were examined by fluorescent microscopy (BZ9000, Keyence, Osaka, Japan).

For cyto-architectural analyses of AVP neurons in the SCN, the SCN was sectionalized into 24 square grids (53 × 53 μm). Five regions were defined; the dorsomedial (DM, 5 grids), centromedial (CM, 4 grids), ventromedial (VM, 5 grids), middle (M, 7 grids) and lateral (L, 3 grids) region. The fluorescence intensity in each

grid was quantified by Aquacosmos (Hamamatsu Photonics) and expressed as difference from the mean intensity of 24 grids. The number of AVP-positive cells in the grids was also counted and compared between the two genotypes.

To confirm the AVP containing cells in bioluminescence spots of the cultured SCN slice, the slices were fixed with PFA after bioluminescence recording and subjected to immunohistochemical staining as mentioned above, except mounting on glass slide, which was done after free-floating staining.

Time-lapse Calcium Imaging

Circadian rhythms in intracellular calcium (Ca^{2+}) level were measured in the cultured SCN on pixel level using time-lapse calcium imaging (Enoki et al., 2012). Aliquots of the adeno-associated virus (AAV, serotype 2/1) (1μl) harboring GCaMP6s, a genetically encoded calcium sensor, under the control of the human synapsin-1 promoter (produced by the University of Pennsylvania Gene Therapy Program Vector Core) were inoculated onto the surface of the cultured SCN slice at 7 days after the preparation from neonatal mice (5 days old; WT, n = 4; $AVP^{ELuc/+}$, n = 5). Infected SCN slices were further cultured for 14 days before imaging. Fluorescence images (2560 × 2160 pixels, 0.325-μm resolution) were captured at an exposure of 2 sec. Images of 100-μm depth in the z axis were obtained at 2 μm z-steps. The imaging system is composed of Nipkow spinning disk confocal (X-Light; Crest Optics), sCMOS CCD camera (NEO; Andor Technology), inverted microscope (Ti-E; Nikon), dry objectives (20 X, 0.75 NA, Plan Apo VC; Nikon), box incubator (TIXHB; Tokai-hit), and MetaMorph software (Molecular Devices). GCaMP6s was excited at cyan color (475/28 nm) with LED light source (Spectra X Light Engine; Lumencor Inc) and the

fluorescence was visualized with 495 nm dichronic mirror and 520/35 nm emission filters (Semlock).

Culture preparation for bioluminescence recording and data analyses

$AVP^{ELuc/+}$ mice of 5-11 months old were sacrificed under LD at ZT 4-8. The brain was harvested in ice-cold Hanks' balanced salt solution.

For a tissue level analysis, four coronal slices of 300 μm thick were prepared from adult mice (n=10) with a microslicer (Dosaka EM, Kyoto, Japan) as described previously (Yoshikawa *et al.*, 2013). The bilateral SCN, PVN, and unilateral SON were dissected from each slice and cultured separately on a membrane (Millicell-CM, Millipore) in DMEM containing 0.1 mM D-luciferin potassium salt and 5% culture supplements, the composition of which is described in Yoshikawa *et al*., (2013). Bioluminescence was recorded for 1 min every 10 min with a photomultiplier tube (PMT) (Lumicycle, Actimetrics; Kronos, Atto, Tokyo, Japan). **Raw data of bioluminescence from day 2 to day 7 in culture was used for evaluation of circadian rhythmicity by Chi-square periodgram (Clock Lab) in the range from 18 to 36 h with a significance level of $p < 0.01$. For determination of the peak phase and amplitude on the tissue level analysis, detrended and smoothed data were used.** Bioluminescent data were detrended by a 24-h moving average subtraction method and then smoothed by a 5-point (SCN) or 11-point (PVN and SON) moving average method. The circadian period was calculated from the interval between successive 3-5 circadian peaks as described previously (Yoshikawa *et al.*, 2013). Amplitude was defined as the difference between the highest and following lowest values of detrended data in a cycle.

In addition, ectopic expression of AVP bioluminescence was examined in several

tissues of the AVP$^{ELuc/+}$ mice (n = 3). The olfactory bulb and median eminence were sliced into 300 μm thick by a microslicer. The anterior pituitary, liver, and lung were hand-sliced with a pair of surgical knives into thin section. The pineal gland was cut halfway through and flattened, and the testis was cut into a small piece. They were subjected to the culture as described above.

For a single cell analysis, 4 coronal slices of 100 μm thick were prepared from adult mice (n = 7) with the microslicer. The slices were trimmed to include the SCN, and cultured on the membranes in DMEM containing 0.2 mM D-luciferin potassium salt at 37°C. Bioluminescence images were obtained using one of the following three CCD cameras cooled to −80 °C: ImagEM (Hamamatsu Photonics, Hamamatsu, Japan), iXon3 (Andor, Belfast, UK), or −60 °C: ORCA II (Hamamatsu Photonics). The images were collected every 60 min (with 59-min exposure) immediately after the start of culture.

Temporal changes in bioluminescence over 72 h were analyzed on the pixel level. A time series of **raw** bioluminescence **data** of each pixel was fitted to a cosine curve, as described previously (Enoki *et al.*, 2012) with minor modifications. Briefly, the pixels in which bioluminescence was less than the background level were excluded from the further analyses. The background level was defined as the mean bioluminescence level of 9 pixels at the darkest corner of an image plus 3 SD of the mean. The best fitted cosine curve was obtained by a least-squares method. The goodness of fit was statistically evaluated by percent rhythm accounted for the fitted cosine wave (Pearson product-moment correlation analysis) at a significance level of $p<0.01$ (Nelson *et al.*, 1979). The first acrophase (circadian peak), amplitude (a double value of mathematical amplitude) and period of the best fitted cosine curve were used as the parameters of

circadian rhythm, and illustrated in pseudocolor.

Contour lines of bioluminescence from isolated cells

The distribution and extent of light signals were evaluated from a single isolated ROI of cell-size surrounded by areas with bioluminescence of the background level. To standardize the bioluminescent image, the background light intensity in each image was subtracted. The background intensity was defined as the mean light intensities of four circles with a 30 μm diameter at the corners of an image plus 3SD of the mean. The circles covered the areas on the tissue outside the SCN. The brightest pixel in the ROI was designated as 100, and the light intensity of pixels around the brightest was expressed as a ratio in 20% bins. Contour analysis was done for the SCN (n = 4 cells from 2 slices) and PVN (n = 3 cells from 2 slices).

Statistical analyses

Differences in the circadian period of behavioral rhythm, in plasma AVP level, and in the intensity of immunohistochemical staining between the WT and transgenic mice were evaluated by the Student's *t* test. Regional differences in parameters of bioluminescence rhythm were evaluated by one-way ANOVA with post-hoc Tukey-Kramer test. A two-way repeated measure or two-factor factorial ANOVA with post-hoc Tukey-Kramer test was used for evaluation of the changes in the circadian phase after a single light pulse, body weight, food/water intake, AVP mRNA expression level, and regional difference in AVP-immunoreactivity and parameters of Ca^{2+} rhythm of both groups of mice.

Results

Body weight, water, and food intake

Body weight was not different between WT (n = 12) and AVP$^{ELuc/+}$ (n = 13) mice from 1 to 10 weeks of age (1 week: WT, 4.1 ± 0.3 g; AVP$^{ELuc/+}$, 4.1 ± 0.6 g. 10 weeks: WT, 23.2 ± 0.9 g; AVP$^{ELuc/+}$, 23.3 ± 1.1 g; mean ± SD). Weekly food and water intake relative to body weight were also not different between WT (n = 5) and AVP$^{ELuc/+}$ (n = 4) mice from 6 to 12 weeks of age (food intake: at 6 weeks, WT, 1.2 ± 0.1 g/g.b.w., AVP$^{ELuc/+}$, 1.1 ± 0.1 g/g.b.w.; at 12 weeks, WT, 0.8 ± 0.0**2** g/g.b.w., AVP$^{ELuc/+}$, 0.8 ± 0.1 g/g.b.w.. water intake: at 6 weeks, WT, 3.1 ± 0.2 g/g.b.w., AVP$^{ELuc/+}$, 3.1 ± 0.4 g/g.b.w.; at 12 week, WT, 2.0 ± 0.3 g/g.b.w., AVP$^{ELuc/+}$, 2.1 ± 0.1 g/g.b.w.).

Formal properties of behavioral rhythm

Formal properties of behavioral rhythm were not significantly different between AVP$^{ELuc/+}$ and wild type littermate (Fig. S1). The free-running circadian period in DD were 23.97 ± 0.02 h (mean ± SD) in WT mice (n = 5) and 23.99 ± 0.02 h in AVP$^{ELuc/+}$ mice (n = 10). A single light pulse given at CT14 and CT22 induced statistically indistinguishable phase-delay (WT, 1.88 ± 0.02 h; AVP$^{ELuc/+}$, 1.77 ± 0.38 h) and phase-advance shifts (WT, 0.54 ± 0.19 h; AVP$^{ELuc/+}$, 0.77 ± 0.40 h) (Fig.S1). The circadian period after the light pulse was 23.83 ± 0.15 h and 23.82 ± 0.10 h in the AVP$^{ELuc/+}$ and littermate WT, respectively.

Spatiotemporal profiles AVP and VIP in the SCN of AVP$^{ELuc/+}$ mice

AVP mRNA expression levels in the SCN, PVN and SON of AVP$^{ELuc/+}$ mice were

comparable with those of WT mice when analyzed by *in situ* hybridization at ZT6 and ZT18 (Fig. 2A, B). Expression level at ZT6 is significantly higher than ZT18 in the SCN of both genotypes ($P< 0.01$, two-factor factorial ANOVA with post-hoc Tukey-Kramer test). No ectopic AVP mRNA expression was found outside the SCN in the coronal brain slice. The distribution of AVP-immunoreactive cells in the SCN of $AVP^{ELuc/+}$ mice (n = 4) was indistinguishable from that of WT mice (n = 4; Fig. 2C, D). The number of AVP-immunoreactive cells in the SCN was not significantly different between $AVP^{ELuc/+}$ (56 ± 3 cells/slice) and WT (52 ± 2 cells/slice) mice. The intensity of AVP-immunostaining was not significantly different between $AVP^{ELuc/+}$ and WT on grid as well as whole tissue level (Fig. 2D). The regional difference in the intensity was detected in both WT and $AVP^{ELuc/+}$ mice between the DM and VM or M region, and between CM and M region ($p<0.01$, one-way ANOVA with post-hoc Tukey-Kramer test).

The intracellular calcium rhythm in the cultured SCN slice was robust in both $AVP^{ELuc/+}$ and WT mice (Fig.2E). Regional distributions of acrophase were not different between them (Fig. 2F, G). In WT mice the circadian peak in the ventral part of the SCN were significantly phase-ahead to the dorsal and central parts ($p<0.05$, $p<0.01$), whereas in $AVP^{ELuc/+}$ mice the circadian peak in the ventral part was significantly phase-ahead only to the central part ($p<0.05$). The difference was mainly due to larger SDs in $AVP^{ELuc/+}$ mice.

Circadian rhythms in bioluminescence

Robust circadian rhythms in AVP-ELuc bioluminescence were detected for more than 10 cycles in the SCN slices (Fig.3A, 4A). The circadian rhythm was stable except

for the initial decline of amplitude. The damping rate in the first 3 cycles was 0.3 ± 0.1 (n=10) and the following cycles (3-10 cycle) was 0.8 ± 0.4 (n = 10). The circadian peak on the first day in culture was located in the middle of the light phase (ZT 4.9 ± 0.5, mean ± SD) and the circadian period was 22.9 ± 0.4 h. AVP-ELuc bioluminescence in the PVN and SON exhibited a large peak on the first day in culture (day 1) and damped immediately. However, circadian rhythms with low amplitude persisted in the subsequent days (Fig. 3A). Chi-square periodogram analysis revealed significant circadian rhythms in 9 PVN of 10 examined, and in 8 SON of 10 examined. The circadian peak on the first day of culture was located at ZT 5.2 ± 1.9 (n = 9) for the PVN and ZT 3.0 ± 2.3 (n = 6) for the SON, respectively (Fig. 3B). The circadian period was 23.0 ± 2.7 h for the PVN and 23.7 ± 2.7 h for the SON. The circadian rhythm in the SCN was more stable in terms of the peak-to-peak variability than those in the PVN and SON. The SD was significantly smaller in the SCN (0.6 ± 0.3, n = 10) than in the PVN (3.7 ± 2.0, n = 6) and SON (5.7 ± 1.7, n = 6) ($p<0.01$, one-way ANOVA with post-hoc Tukey-Kramer test).

Only low basal levels of bioluminescence were detected in the cultured olfactory bulb, median eminence, anterior pituitary, pineal gland, liver, lung, and testis **of the** $AVP^{ELuc/+}$ mice (n = 3, **Fig. S3)**.

Bioluminescence imaging with a CCD camera revealed that AVP-ELuc expressed cells were sporadically scattered in the shell region of the SCN (Fig. 4B, 5A). Circadian rhythms in sell-sized region of interest (ROI) were analyzed (Fig.4C, Fig.5B). The mean number of ROI in each slice was 36.4 ± 14.9 (n=7). The variability of the rhythm was assessed by comparing SD of the peak-to-peak intervals of each ROI with that of the whole SCN of the same slice. Three consecutive peak-to-peak intervals (day1-4 in

culture) were calculated and SD of the intervals was obtained in each SCN slice and ROIs contained in it. The variability was significantly larger in ROI than in the whole SCN in 5 out of 7 slices examined ($P<0.01$, t-test), suggesting that the circadian rhythm is more stable on tissue level than on cellular level.

A simple summation of circadian rhythms in ROIs reproduced only a fraction of the circadian amplitude on the whole SCN level (Fig. 4C), indicating that the circadian rhythms in other areas than identified ROIs greatly contributed to the shape of circadian rhythm on tissue level. To increase the resolution of circadian rhythm analysis, we used a cosine curve fitting method on pixel level (Enoki *et al.*, 2012). The pixel level analysis revealed the distribution of circadian AVP rhythm in the SCN, showing regional specificities in the acrophase (circadian peak), amplitude and circadian period (Fig. 5D, S2A). The distribution of bioluminescence was in good agreement with immunohistochemically stained AVP areas (Fig. 5C, S2C). A ratio of the numbers of AVP-Eluc cells and AVP-immunopositive sells in the outermost focal plane of an SCN slice was 92.7 ± 9.3 % (n=3). The acrophases and amplitude of AVP circadian rhythms in the dorsomedial and ventromedial areas were markedly different from the centromedial area, whereas no regional difference was detected in the period and percent rhythm, an index of the curve fitting accuracy (Fig. S2B). These findings indicate the existence of at least two distinct regional clusters of AVP circadian rhythms.

Contour lines of bioluminescence from isolated cells

The distribution and extent of bioluminescence signals was examined in a single isolated ROI in the SCN and PVN (Fig. 6A). The area covered by pixels emitting the luminescence was slightly larger in the peak phase (brightest) than in the trough

phase (dimmest) in the PVN, but was not much different in the SCN (Fig. 6B). The intensity of bioluminescence reduced linearly along with the distance from the brightest center (Fig. 6B). The level of bioluminescence in a single ROI was expressed by contours in 20 % bins, where the brightest pixel represented 100%. The size of area enclosed by each contour is plotted against bioluminescence brightness in a cumulative manner. The size correlated significantly with brightness (SCN, dim, $y = 15.6x - 21.6$, $r = 0.992$; bright, $y = 20.3x - 34.6$, $r = 0.986$; PVN, dim, $y = 83.5x - 135.8$, $r = 0.999$; bright, $y = 82.4x - 107.0$, $r = 0.997$). The regressions were all statistically significant ($p<0.01$). The area where a regression line reaches 0 % of brightness is assumed to the limit of bioluminescence radiation. The mean area of isolated ROI so far detected in the SCN (bright, 89 $\pm$ 13; dim 71 $\pm$ 10 μm^2, $n = 4$) and in the PVN (bright, 376 $\pm$ 28; dim 343 $\pm$ 38 μm^2, $n = 3$) were almost identical to the size of SCN (van den Pol, 1991) and PVN neurons (Sofroniew, 1985).

Discussion

We successfully monitored circadian rhythms in AVP-ELuc bioluminescence not only from the SCN but also from the PVN and SON slices in culture, indicating that a bioluminescence reporter of newly developed AVP^{ELuc} knock-in mice is useful. $AVP^{ELuc/+}$ mice exhibited circadian behavior rhythms indistinguishable from those of WT mice in free-running periods in DD and in phase responses to a single light pulse, indicating that gene manipulation did not disturb the circadian system (Fig. S1). In addition, the configurative profile of AVP neurons as well as the expression level of AVP in the SCN was not different between $AVP^{ELuc/+}$ and WT mice (Fig. 2A-D). The

same was essentially the case for the circadian rhythm in intracellular Ca^{2+} concentration on pixel level (Fig.2E-G). All these results indicated that a single allele of AVP gene produces AVP sufficient to keep physiological functions.

Circadian rhythms in bioluminescence were detected in the SCN slices, and the peak phase was located in the middle of the light phase of LD 12:12 (Fig. 3, 4A). The peak phase is similar to SCN culture of *Period1-luciferase* transgenic mouse (Inagaki *et al.*, 2007) and approximately 6 h phase advance from that of *Period2*^{Luiferasec} knock-in mouse (Yoo *et al.*, 2004). Circadian peaks of AVP mRNA level in the SCN was reported to be in the late light phase in mice (Burbach *et al.*, 1988; Cagampang *et al.*, 1994; Dardente *et al.*, 2004; Maruyama *et al.*, 2010) and rats (Burbach *et al.*, 1988; Cagampang *et al.*, 1994; Maruyama *et al.*, 2010). The circadian peak of AVP heteronuclear (hn) RNA expression preceded the peak of AVP mRNA, indicating a time lag between AVP transcription and the peak mRNA level (Maruyama *et al.*, 2010). AVP peptide in the rat SCN peaked in the first half (Södersten *et al.*, 1985; Tominaga *et al.*, 1992) or the second half of the light phase (Yamase *et al.*, 1991) or in a bimodal pattern (Noto *et al.*, 1983). Diurnal variation in the AVP level was reported in the PVN and SON (Noto *et al.*, 1983), whereas no rhythmic expression of AVP mRNA was found in these nuclei (Burbach *et al.*, 1988; Cagampang *et al.*, 1994; Dzirbíková *et al.*, 2011). Daily variation was reported in the length of the polyA tail of the AVP mRNA in SCN but not in the PVN and SON (Robinson *et al.*, 1988), which may explain the difference in the AVP expression pattern ~~of~~ between the SCN and the PVN or the SON (Garbarino-Pico & Green, 2007). Discrepancy among these previous studies may be due to the sampling intervals, which were mostly at 4 h. As for the SCN, the present results are consistent with the results of AVP hnRNA expression (Maruyama *et al.*, 2010).

The stability of cellular AVP-ELuc rhythm in terms of the variability of peak phase or peak-to-peak intervals is less than that of SCN slice rhythm (Fig. 4D). Similar instability in cellular rhythms has been reported in electric activity (Welsh et al, 1995; Honma et al., 2004, Herzog et al., 2004) and clock gene expression (Yamaguchi *et al.*, 2003). In *ex vivo* conditions, the cellular coupling of circadian oscillation would decrease and the variability in phase or period of cellular rhythm would increase. On the other hand, the SCN slice rhythm may keep its stability, because it is the integrated or summated rhythm of cellular circadian rhythms.

A simple summation of cellular rhythms in ROIs showed a similar profile of the circadian rhythm in the whole SCN slice but reproduced only a fraction of amplitude actually measured (Fig. 4C). The discrepancy is probably related to the fact that bioluminescence from an AVP-ELuc cell deep inside the SCN slice substantially decay when passing through the tissue (Yizhar *et al.*, 2011). Whatever the reason might be, a number of cellular circadian rhythms with low amplitude contribute to the SCN circadian rhythm in a slice. Therefore, a result based only on a small number of ROI rhythms should be carefully interpreted.

A cosine curve fitting method on a pixel level proved the above possibility by showing a large AVP oscillation area essentially identical to the immunoreactive AVP area in the SCN (Fig. 5C). In addition, the method revealed the spatial distribution of AVP cellular circadian rhythms with different phases, amplitudes and periods. The acrophase-map indicated that the mean acrophase in the dorsomedial and ventromedial areas were similar to each other but significantly different from that in the centromedial area (Fig.5D, S2B). These findings are consistent with previous reports on regional differences in the circadian phases of clock gene expression (Nagano *et al.*, 2003;

Yamaguchi *et al.*, 2003; Evans *et al.*, 2011), AVP gene expression (Hamada *et al.*, 2004) and Ca^{2+} concentration (Enoki *et al.*, 2012), indicating phase-advance in the dorsomedial area relative to the ventromedial area. The present study indicates that there are at least two regionally specific clusters of AVP circadian oscillation in the SCN. However, mechanism and functions of the different AVP clusters wait elucidation.

The large peak in the first cycle of culture in the PVN and SON was not an artifact but seemed to be a true circadian peak, because the peak phase was not statistically different from the extrapolated peak phase from a regression line fitted to the circadian peaks in the later cycles. It remains to be shown the reason for the initial damping of amplitude.

It is a matter of debate how exactly the intensity of bioluminescence reflects transcription activity of a gene (Foley *et al.*, 2011). We tried to answer this question using an isolated ROI on the pixel level. The two-dimensional distribution of light intensity around the brightest pixel revealed the area corresponded to an average size of a single cell in both the SCN and PVN (Fig. 6). The finding was based on the analysis of smallest ROI, which might exclude overlapping of cells. Actually, an area of a larger ROI was double or triple in size of a smallest one, suggesting overlapping of more than one cell. The size of the luminescent area was essentially the same in the peak (brightest) and trough (dimmest) phase, indicating that a bioluminescence profile reflects the distribution of emitting cells.

We conclude that AVP gene expression in cultured mouse SCN shows robust circadian rhythms, peaking in the middle of the subjective day. The area where circadian rhythms in AVP expression were recognized in the SCN on pixel level was essentially

identical to the area determined immunohistochemically. AVP expression in the PVN and SON also exhibited circadian rhythms which were not as stable as in the SCN, suggesting a strong influence of the SCN circadian pacemaker on these nuclei. The formal property of behavior rhythm as well as the SCN cytoarchitecture of the AVP^{ELuc} knock-in mice was indistinguishable from those of WT. The AVP^{ELuc} mice will be useful not only for circadian but also for neuroendocrinological studies.

Acknowledgements

We thank Dr. Y. Ueta (University of Occupational and Environmental Health) for his valuable suggestions, which enabled us to generate AVP^{ELuc} knock-in mice. We also thank Dr. A. Wirz-Justice for her critical reading of our manuscript, Dr. H. Gainer (National Institutes of Health) for the generous donation of AVP antibody for immunohistochemistry, and Drs. G.J. Boer and J.J. van Heerikhuize (the Netherlands Institute for Brain Research) for the donation of AVP antiserum for radioimmunoassay. We thank the Genetically-Encoded Neuronal Indicator and Effector (GENIE) Project and the Janelia Farm Research Campus of the Howard Hughes Medical Institute for sharing GCaMP6 constructs. We appreciate the technical assistance of Ms. M. Shudo, Y. Suzuki, and M. Fukiya.

This work was supported in part by Grant-in-Aid for Scientific Research (B) (No.24390055 to S.H.) from Japan Society for the Promotion of Science (JSPS), Grant-in-Aid for Scientific Research (A) (No. 20249010 to K.H.) from JSPS, Cooperative Research Project for Advanced Photonic Bioimaging from the ministry of Education, Culture, Sports, Science and Technology of Japan (MEXT), Project for

Creation of Innovation Centers for Advanced Interdisciplinary Research Areas Program from JSPS, and Grant-in-Aid for Scientific Research on Priority Areas-Integrative Brain Research (No.200119002) from MEXT.

References

Baba, K., Ono, D., Honma, S. & Honma, K.-i. (2008) A TTX-sensitive local circuit is involved in the expression of PK2 and BDNF circadian rhythms in the mouse suprachiasmatic nucleus. *Eur. J. Neurosci.*, **27**, 909-916.

Ban, Y., Shigeyoshi, Y. & Okamura, H. (1997) Development of Vasoactive Intestinal Peptide mRNA Rhythm in the Rat Suprachiasmatic Nucleus. *J. Neurosci.*, **17**, 3920-3931.

Burbach, J.P.H., Liu, B., Voorhuis, T.A.M. & Van Tol, H.H.M. (1988) Diurnal variation in vasopressin and oxytocin messenger RNAs in hypothalamic nuclei of the rat. *Mol. Brain Res.*, **4**, 157-160.

Cagampang, F.R.A., Yang, J., Nakayama, Y., Fukuhara, C. & Inouye, S.-I.T. (1994) Circadian variation of arginine-vasopressin messenger RNA in the rat suprachiasmatic nucleus. *Mol. Brain Res.*, **24**, 179-184.

Dardente, H., Menet, J.S., Challet, E., Tournier, B.B., Pévet, P. & Masson-Pévet, M. (2004) Daily and circadian expression of neuropeptides in the suprachiasmatic nuclei of nocturnal and diurnal rodents. *Mol. Brain Res.*, **124**, 143-151.

Dzirbíková, Z., Kiss, A., Okuliarová, M., Kopkan, L., Červenka, L. & Zeman, M. (2011) Expressions of per1 Clock Gene and Genes of Signaling Peptides Vasopressin, Vasoactive Intestinal Peptide, and Oxytocin in the Suprachiasmatic and Paraventricular Nuclei of Hypertensive TGR[mREN2]27 Rats. *Cell. Mol. Neurobiol.*, **31**, 225-232.

Enoki, R., Kuroda, S., Ono, D., Hasan, M.T., Ueda, T., Honma, S. & Honma, K.-i. (2012) Topological specificity and hierarchical network of the circadian calcium rhythm in the suprachiasmatic nucleus. *Proc. Natl. Acad. Sci. U. S. A.*, **109**, 21498-21503.

Evans, J.A., Leise, T.L., Castanon-Cervantes, O. & Davidson, A.J. (2011) Intrinsic Regulation of Spatiotemporal Organization within the Suprachiasmatic Nucleus. *PLoS One*, **6**, e15869.

Foley, N.C., Tong, T.Y., Foley, D., LeSauter, J., Welsh, D.K. & Silver, R. (2011) Characterization of orderly spatiotemporal patterns of clock gene activation in mammalian suprachiasmatic nucleus. *Eur. J. Neurosci.*, **33**, 1851-1865.

Francl, J.M., Kaur, G. & Glass, J.D. (2010) Regulation of vasoactive intestinal polypeptide release in the SCN circadian clock. *Neuroreport*, **21**, 1055-1059.

Fukaya, M., Tsujita, M., Yamazaki, M., Kushiya, E., Abe, M., Akashi, K., Natsume, R., Kano, M., Kamiya, H., Watanabe, M. & Sakimura, K. (2006) Abundant distribution of TARP γ-8 in synaptic and extrasynaptic surface of hippocampal neurons and its major role in AMPA receptor expression on spines and dendrites. *Eur. J. Neurosci.*, **24**, 2177-2190.

Garbarino-Pico, E. & Green, C.B. (2007) Posttranscriptional Regulation of Mammalian Circadian Clock Output. *Cold Spring Harb. Symp. Quant. Biol.*, **72**, 145-156.

Hamada, T., Antle, M.C. & Silver, R. (2004) Temporal and spatial expression patterns of canonical clock genes and clock-controlled genes in the suprachiasmatic nucleus. *Eur. J. Neurosci.*, **19**, 1741-1748.

Herzog, E.D., Aton, S.J., Numano, R., Sakaki, Y. & Tei, H. (2004) Temporal Precision in the Mammalian Circadian System: A Reliable Clock from Less Reliable Neurons. *J. Biol. Rhythms*, **19**, 35-46.

Honma, S., Nakamura, W., Shirakawa, T. & Honma, K.-i. (2004) Diversity in the circadian periods of single neurons of the rat suprachiasmatic nucleus depends on nuclear structure and intrinsic period. *Neurosci. Lett.*, **358**, 173-176.

Inagaki, N., Honma, S., Ono, D., Tanahashi, Y. & Honma, K. (2007) Separate oscillating cell groups in mouse suprachiasmatic nucleus couple photoperiodically to the onset and end of daily activity. *Proc. Natl. Acad. Sci. U. S. A.*, **104**, 7664-7669.

Iovino, M., Guastamacchia, E., Giagulli, V.A., Licchelli, B. & Triggiani, V. (2012) Vasopressin secretion control: central neural pathways, neurotransmitters and effects of drugs. *Curr. Pharm. Des.*, **18**, 4714-4724.

Kalsbeek, A., Fliers, E., Hofman, M.A., Swaab, D.F. & Buijs, R.M. (2010) Vasopressin and the Output of the Hypothalamic Biological Clock. *J. Neuroendocrinol.*, **22**, 362-372.

Maruyama, T., Ohbuchi, T., Fujihara, H., Shibata, M., Mori, K., Murphy, D., Dayanithi, G. & Ueta, Y. (2010) Diurnal changes of arginine vasopressin-enhanced green fluorescent protein fusion transgene expression in the rat suprachiasmatic nucleus. *Peptides*, **31**, 2089-2093.

Mieda, M., Ono, D., Hasegawa, E., Okamoto, H., Honma, K.-i., Honma, S. & Sakurai, T. (2015) Cellular Clocks in AVP Neurons of the SCN Are Critical for Interneuronal Coupling Regulating Circadian Behavior Rhythm. *Neuron*, **85**, 1103-1116.

Millar, A.J., Short, S.R., Chua, N.H. & Kay, S.A. (1992) A novel circadian phenotype based on firefly luciferase expression in transgenic plants. *Plant Cell*, **4**, 1075-1087.

Mishina, M. & Sakimura, K. (2007) Conditional gene targeting on the pure C57BL/6 genetic background. *Neurosci. Res.*, **58**, 105-112.

Moore, R.Y., Speh, J.C. & Leak, R.K. (2002) Suprachiasmatic nucleus organization. *Cell Tissue Res.*, **309**, 89-98.

Nagano, M., Adachi, A., Nakahama, K.-i., Nakamura, T., Tamada, M., Meyer-Bernstein, E., Sehgal, A. & Shigeyoshi, Y. (2003) An abrupt shift in the day/night cycle causes desynchrony in the mammalian circadian center. *J. Neurosci.*, **23**, 6141-6151.

Nakajima, Y., Yamazaki, T., Nishii, S., Noguchi, T., Hoshino, H., Niwa, K., Viviani, V.R. & Ohmiya, Y. (2010) Enhanced beetle luciferase for high-resolution bioluminescence imaging. *PloS one*, **5**, e10011.

Nelson, W., Tong, Y.L., Lee, J.K. & Halberg, F. (1979) Methods for cosinor-rhythmometry. *Chronobiologia.*, **6**, 305-323.

Nishide, S., Honma, S., Nakajima, Y., Ikeda, M., Baba, K., Ohmiya, Y. & Honma, K. (2006) New reporter system for *Per1* and *Bmal1* expressions revealed self-sustained circadian rhythms in peripheral tissues. *Genes Cells*, **11**, 1173-1182.

Noto, T., Hashimoto, H., Doi, Y., Nakajima, T. & Kato, N. (1983) Biorhythm of arginine-vasopressin in the paraventricular, supraoptic and suprachiasmatic nuclei of rats. *Peptides*, **4**, 875-878.

Robinson, B.G., Frim, D.M., Schwartz, W.J. & Majzoub, J.A. (1988) Vasopressin mRNA in the suprachiasmatic nuclei: daily regulation of polyadenylate tail length. *Science*, **241**, 342-344.

Romijn, H.J., Sluiter, A.A., Pool, C.W., Wortel, J. & Buijs, R.M. (1997) Evidence from confocal fluorescence microscopy for a dense, reciprocal innervation between AVP-, somatostatin-, VIP/PHI-, GRP- and VIP/PHI/GRP-immunoreactive neurons in the rat suprachiasmatic nucleus. *Eur. J. Neurosci.*, **9**, 2613-2623.

Rood, B.D. & De Vries, G.J. (2011) Vasopressin innervation of the mouse (Mus musculus) brain and spinal cord. *J. Comp. Neurol.*, **519**, 2434-2474.

Södersten, P., De Vries, G.J., Buijs, R.M. & Melin, P. (1985) A daily rhythm in behavioral vasopressin sensitivity and brain vasopressin concentrations. *Neurosci. Lett.*, **58**, 37-41.

Schwartz, W.J. & Reppert, S.M. (1985) Neural regulation of the circadian vasopressin rhythm in cerebrospinal fluid: a pre-eminent role for the suprachiasmatic nuclei. *J. Neurosci.*, **5**, 2771-2778.

Shinohara, K., Honma, S., Katsuno, Y., Abe, H. & Honma, K. (1995) Two distinct oscillators in the rat suprachiasmatic nucleus in vitro. *Proc. Natl. Acad. Sci. U. S. A.*, **92**, 7396-7400.

Shinohara, K., Tominaga, K., Isobe, Y. & Inouye, S.T. (1993) Photic regulation of peptides located in the ventrolateral subdivision of the suprachiasmatic nucleus of the rat: daily variations of vasoactive intestinal polypeptide, gastrin-releasing peptide, and neuropeptide Y. *J. Neurosci.*, **13**, 793-800.

Sofroniew, M.V. (1985) Vasopressin- and neurophysin-immunoreactive neurons in the septal region, medial amygdala and locus coeruleus in colchicine-treated rats. *Neuroscience*, **15**, 347-358.

Tominaga, K., Shinohara, K., Otori, Y., Fukuhara, C. & Inouye, S.T. (1992) Circadian rhythms of vasopressin content in the suprachiasmatic nucleus of the rat. *Neuroreport*, **3**, 809-812.

Ueta, Y., Fujihara, H., Serino, R., Dayanithi, G., Ozawa, H., Matsuda, K.-i., Kawata, M., Yamada, J., Ueno, S., Fukuda, A. & Murphy, D. (2005) Transgenic Expression of Enhanced Green Fluorescent Protein Enables Direct Visualization for Physiological Studies of Vasopressin Neurons and Isolated Nerve Terminals of the Rat. *Endocrinology*, **146**, 406-413.

van den Pol, A. (1991) The suprachiasmatic nucleus: Morphological and cytochemical substrates for cellular interaction. In Klein DC, M.R., Reppert SM (ed) *Suprachiasmatic nucleus*. Oxford University Press, New York, pp. 17-50.

Welsh, D.K., Logothetis, D.E., Meister, M. & Reppert, S.M. (1995) Individual neurons dissociated from rat suprachiasmatic nucleus express independently phased circadian firing rhythms. *Neuron*, **14**, 697-706.

Yamaguchi, S., Isejima, H., Matsuo, T., Okura, R., Yagita, K., Kobayashi, M. & Okamura, H. (2003) Synchronization of Cellular Clocks in the Suprachiasmatic Nucleus. *Science*, **302**, 1408-1412.

Yamaguchi, Y., Suzuki, T., Mizoro, Y., Kori, H., Okada, K., Chen, Y., Fustin, J.-M., Yamazaki, F., Mizuguchi, N., Zhang, J., Dong, X., Tsujimoto, G., Okuno, Y., Doi, M. & Okamura, H. (2013) Mice Genetically Deficient in Vasopressin V1a and V1b Receptors Are Resistant to Jet Lag. *Science*, **342**, 85-90.

Yamase, K., Takahashi, S., Nomura, K., Haruta, K. & Kawashima, S. (1991) Circadian changes in arginine vasopressin level in the suprachiasmatic nuclei in the rat.

Neurosci. Lett., **130**, 255-258.

Yasunaga, M., Murotomi, K., Abe, H., Yamazaki, T., Nishii, S., Ohbayashi, T., Oshimura, M., Noguchi, T., Niwa, K., Ohmiya, Y. & Nakajima, Y. (2015) Highly sensitive luciferase reporter assay using a potent destabilization sequence of calpain 3. *J. Biotechnol.*, **194**, 115-123.

Yizhar, O., Fenno, Lief E., Davidson, Thomas J., Mogri, M. & Deisseroth, K. (2011) Optogenetics in Neural Systems. *Neuron*, **71**, 9-34.

Yoo, S.-H., Yamazaki, S., Lowrey, P.L., Shimomura, K., Ko, C.H., Buhr, E.D., Siepka, S.M., Hong, H.-K., Oh, W.J., Yoo, O.J., Menaker, M. & Takahashi, J.S. (2004) PERIOD2::LUCIFERASE real-time reporting of circadian dynamics reveals persistent circadian oscillations in mouse peripheral tissues. *Proc. Natl. Acad. Sci. U. S. A.*, **101**, 5339-5346.

Yoshikawa, T., Matsuno, A., Yamanaka, Y., Nishide, S.-y., Honma, S. & Honma, K.-i. (2013) Daily exposure to cold phase-shifts the circadian clock of neonatal rats in vivo. *Eur. J. Neurosci.*, **37**, 491-497.

Figure legend

Figure 1. Generation of AVP^{ELuc} knock-in mice

A. Gene construct of emerald-luciferase (ELuc) along with PEST, SV40, and poly A sequences. The ELuc-Neo construct was knocked-in into the mouse *AVP* locus. Gray boxes indicate AVP coding region spanning exons 1-3. The open box just upstream of the coding region indicates the 5′ untranslated region. The pgk-gb2 neomycin resistance sequence (Neo) was flanked by Flp recombination target sites. Wave lines indicate probes used for Southern blotting. Abbreviations: Met, initial methionine; DT, diphtheria toxin A-chain cassette; B, BamH I; K, Kpn I. **B.** Southern blotting of genomic DNA from wild-type (WT) and the knock-in (KI) ES clone used for the generation of chimeric mice. Homologous recombinants were identified under the following conditions: Kpn I-digested genomic DNA hybridized with a 5′ probe, 7.9 kb for WT and 11.4 kb for the targeted allele; Kpn I digestion and neo probe; 11.4 kb for targeted allele; BamH I digestion and 3′ probe, 10.9 kb for WT and 14.6 kb for the targeted allele. **C**. Result of PCR genotyping. N, no template control; Het, $AVP^{ELuc/+}$; Homo, $AVP^{ELuc/Eluc}$; M, DNA molecular weight marker.

Figure 2. A. Representative autoradiograms of AVP mRNA expression in the SCN, PVN and SON in the frontal plane. Autoradiographic images are overlaid with crystal violet staining images in pale grey to orientate the brain areas. Scale bar indicates 2 mm. **B.** AVP mRNA expression levels in the SCN, PVN and SON at ZT6 (WT, n = 5; $AVP^{ELuc/+}$, n = 6) and ZT18 (WT, n = 5; $AVP^{ELuc/+}$, n = 4). Open and closed bars indicate the results from WT and $AVP^{ELuc/+}$ mice, respectively. Values are expressed as mean ±

SD. Asterisks (*) indicate statistically significant differences ($P < 0.01$, two-factor factorial ANOVA with post-hoc Tukey–Kramer test). **C.** Representative immunofluoromicrographs of AVP (red) and VIP (green) in the SCN from WT and $AVP^{ELuc/+}$ mice. Scale bar indicates 100 μm. III indicates the third ventricle and OC the optic chiasm. **D.** The mean (upper) and SD (lower) of AVP immunofluorescence intensities (n = 4) in arbitrary unit (a.u) standardized as a difference from the slice mean are demonstrated with pseudocolors in 24 grids. The SCN slice was sectionized into 5 regions demarcated by broken lines of different colors (red, DM; green, CM; blue, VM; orange, M; purple, L; **shown in left lower panel**). No significant difference is detected between WT and $AVP^{ELuc/+}$ for corresponding grids in two dimensional coordinates. **E.** Representative circadian rhythms of intracellular Ca^{2+} level in the cultured SCN slice from WT and $AVP^{ELuc/+}$ mice. Circadian rhythms in the dorsal (D), central (C) and ventral (V) regions of the SCN are expressed in different color. **F.** Representative acrophase maps on pixel level of the circadian Ca^{2+} rhythm in the cultured SCN slices from WT and $AVP^{ELuc/+}$ mice. A scale of pseudocolor indicates relative time to the slice mean defined as 12 h. **G.** The mean acrophases of circadian Ca^{2+} rhythm from three different regions of the SCN (enclosed by white lines in Fig. 2F). Open and closed color circles indicate the results of WT (n = 4) and $AVP^{ELuc/+}$ (n = 5) mice, respectively. No significant difference is detected between WT and $AVP^{ELuc/+}$, while regional differences are detected (*, $P < 0.05$; **, $P < 0.01$, V vs. D or C, two-way repeated measure ANOVA with post-hoc Tukey–Kramer test).

Figure 3. Circadian AVP-ELuc rhythms in cultured brain slices on tissue level

A. Representative circadian AVP-ELuc rhythms in the cultured SCN (top), PVN

(middle) and SON (bottom) slices of $AVP^{ELuc/+}$ mice. Grey line indicates raw data. Black line indicates detrended data. Chi-square periodogram (right) indicates significant circadian rhythms from day 2 to 7 in culture. An oblique broken line in the periodogram indicates a significance level ($P<0.01$). **B.** Mean peak phases of circadian AVP-ELuc rhythm on the first cycle in the cultured SCN (n = 9), PVN (n = 9) and SON (n = 6) slices. The values were expressed in the mean ± SD. The abscissa indicates the time of day in ZT, immediately before culturing.

Figure 4. Circadian AVP-ELuc rhythm in the cultured SCN of $AVP^{ELuc/+}$ mice

A. Circadian AVP-ELuc rhythms in the SCN slices of $AVP^{ELuc/+}$ mice (n = 5). Each line indicates the circadian rhythm from a different SCN slice. **B.** Bright field image at the beginning of bioluminescence recording by a CCD camera. Colored dots indicate the position of ROIs, the circadian AVP-ELuc rhythms of which are shown in a panel C. Yellow dashed lines indicate the margin of the SCN identified by DAPI staining. **III** indicates the third ventricle, and OC the optic chiasm. Scale bar indicates 200 μm. **C.** Circadian AVP-ELuc rhythm in an SCN slice. Each line represents circadian AVP-ELuc rhythm in a ROI (n = 34) corresponding to the colored dot in B. Blue thick line in the panel indicates the sum of bioluminescence in the ROIs examined and red thick line indicates the sum of bioluminescence of the whole SCN slice. A white and black horizontal bar at the bottom of each panel indicates a light and dark cycle on the day of brain preparation. **D.** Variability in the period of circadian AVP-ELuc rhythm in terms of the peak-to-peak intervals on SCN tissue and cell levels. SDs of the intervals in 7 SCN slices are indicated in the left and the mean intervals of ROIs in each SCN slice were indicated by circles with vertical lines (SD). The same color indicates the results from

the same slice. The mean SD on ROI level was significantly larger than SD on tissue level in 5 out of 7 SCN slices. Asterisk (*) indicate a statistically significant difference ($P<0.01$, t-test).

Figure 5. Bioluminescence images and a pixel-level analysis of circadian AVP-ELuc rhythm in the cultured SCN

A. Bioluminescence images are illustrated in pseudocolor at every 4 h interval on day 8 in culture. Numbers at the right corner indicate local time when the image was acquired. Unilateral right SCN is shown, and a yellow dashed line indicates the margin of the SCN identified by DAPI staining. Letters in the lower right panel indicate ROIs, circadian bioluminescence rhythms of which are illustrated in the panel C. Scale bar indicates 100 μm. OC, optic chiasm; III, the third ventricle. **B.** Circadian AVP-ELuc rhythm**s** of 7 representative cells in an SCN slice are illustrated for 3.5 cycles with different colors (a-g in A). Culture medium was exchanged at times indicated by an arrow. **C.** Immunohistochemical staining after bioluminescence recording of the same SCN slice as A (scale bar, 100 μm). Immunopositive signals with anti-AVP and anti-VIP are shown in red and green, respectively. Arrows with alphabets indicate the same ROIs as in A (a-g). The margin of the SCN is indicated by a yellow dashed line. Cells designated as a, c, d and g are shown on the right panels with a higher magnification (scale bar, 25 μm). **D.** Pixel-level demonstration of circadian parameters of bioluminescence rhythm illustrated in A; acrophase, amplitude, period and percent rhythm (PR) in pseudocolors. Color scale of acrophase indicates relative time to the slice mean defined as 12 h. Goodness of curve fitting is indicated by PR: highest with 1 and lowest with 0. The limit of significance for fitting is shown at the scale bar by a

triangle. Pixels with bioluminescence intensity less than the background level are indicated with **white** color and aperiodic pixels are indicated with black color. The margin of the SCN is indicated by yellow dashed line and ROIs examined (a-g, same as in A) are indicated by **letters**. III, third ventricle; OC, optic chiasm. Scale bars indicate 100 μm.

Figure 6. Contour analysis of an isolated ROI in the SCN and PVN

A. Representative contour lines of bioluminescence from an isolated cell-sized ROI in the SCN (upper) and PVN (lower) at the dim (left) and bright (right) phases of circadian rhythm. Different levels of contour are expressed relative to the highest level by different colors in 20 % bins. Scale bars indicate 3.7 μm. **B.** The size of area enclosed by each contour is plotted against the ratio of brightest bioluminescence (%) in a cumulative manner. The values are expressed with the mean and SD (SCN, n = 4: PVN, n = 3). The area where a vertical liner line on 0 % (dashed line) hits is assumed to the limit of bioluminescence radiation.

Fig. 1

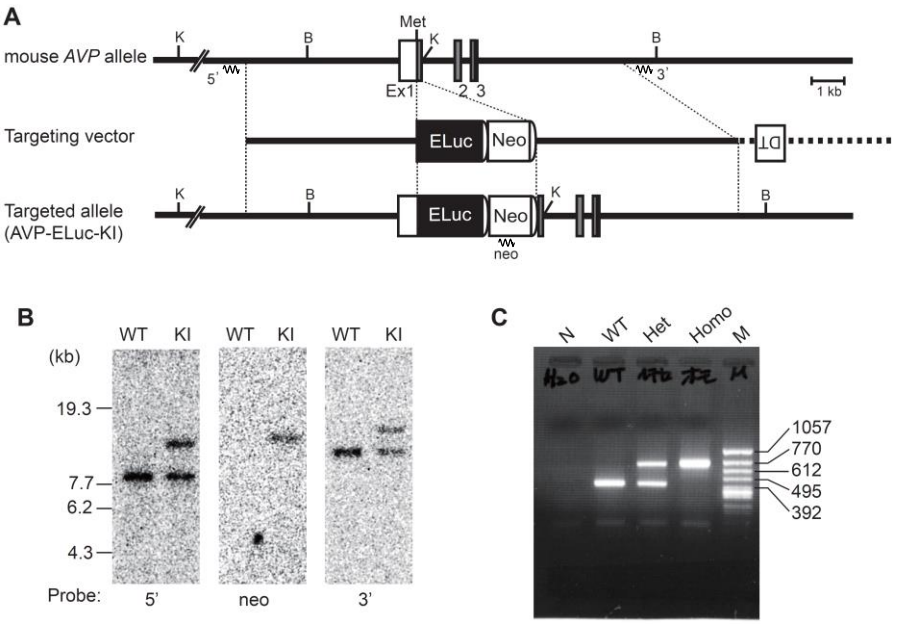
A
mouse AVP allele
K
B
Met
K
B
5'
Ex1
2 3
3'
1 kb
Targeting vector
ELuc
Neo
DT
Targeted allele
(AVP-ELuc-KI)
K
B
ELuc
Neo
K
B
neo
B
WT KI WT KI WT KI
(kb)
19.3
7.7
6.2
4.3
Probe:
5'
neo
3'
C
N
WT
Het
Homo
M
1057
770
612
495
392

Fig. 2

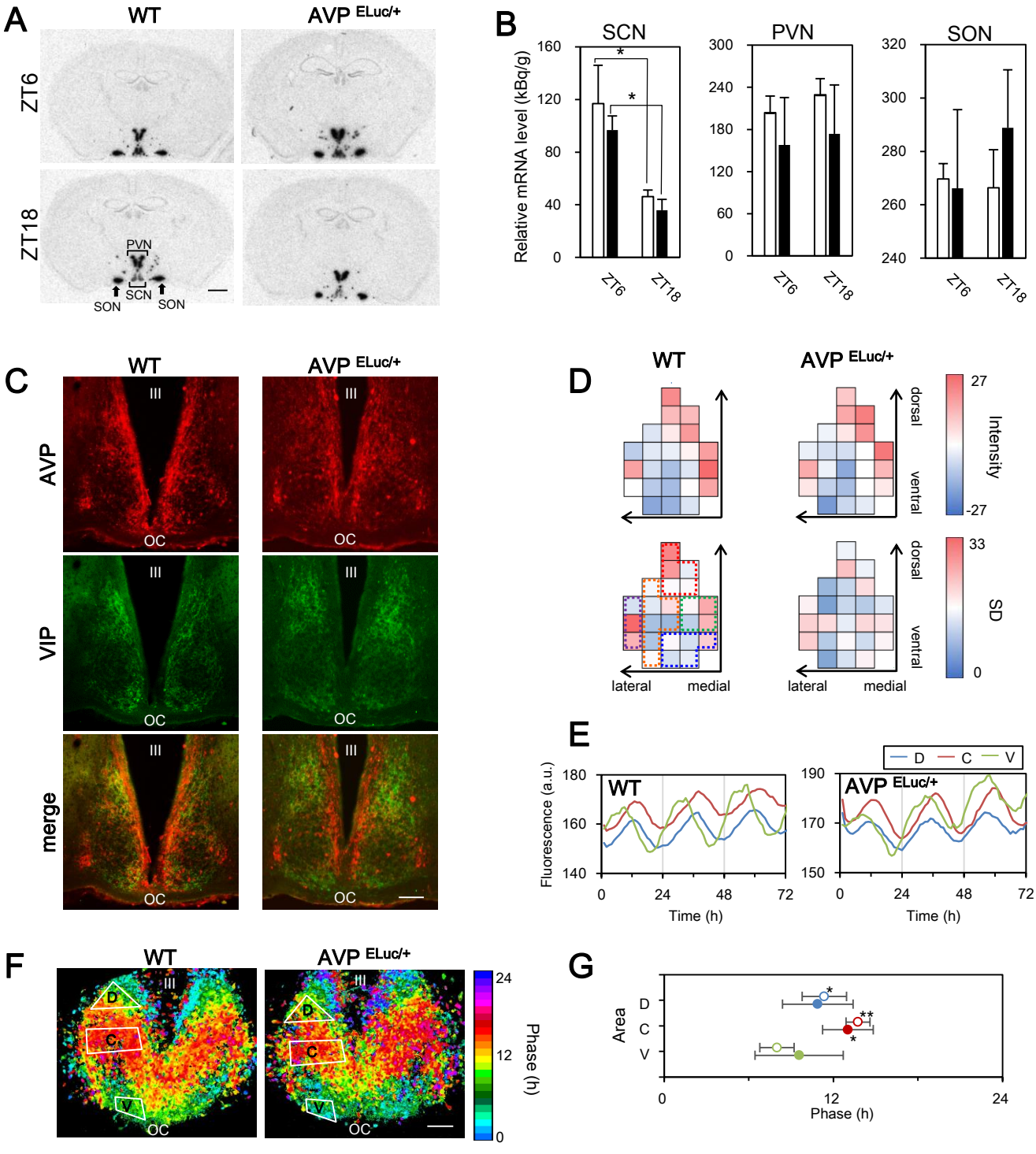
A
WT
AVP ELuc/+
ZT6
ZT18
PVN
SCN
SON
SON
B
SCN
PVN
SON
Relative mRNA level (kBq/g)
ZT6
ZT18
C
WT
AVP ELuc/+
AVP
VIP
merge
III
OC
D
WT
AVP ELuc/+
dorsal
ventral
lateral
medial
Intensity
SD
E
WT
AVP ELuc/+
D
C
V
Fluorescence (a.u.)
Time (h)
F
WT
AVP ELuc/+
D
C
V
OC
Phase (h)
G
Area
Phase (h)

Fig. 3

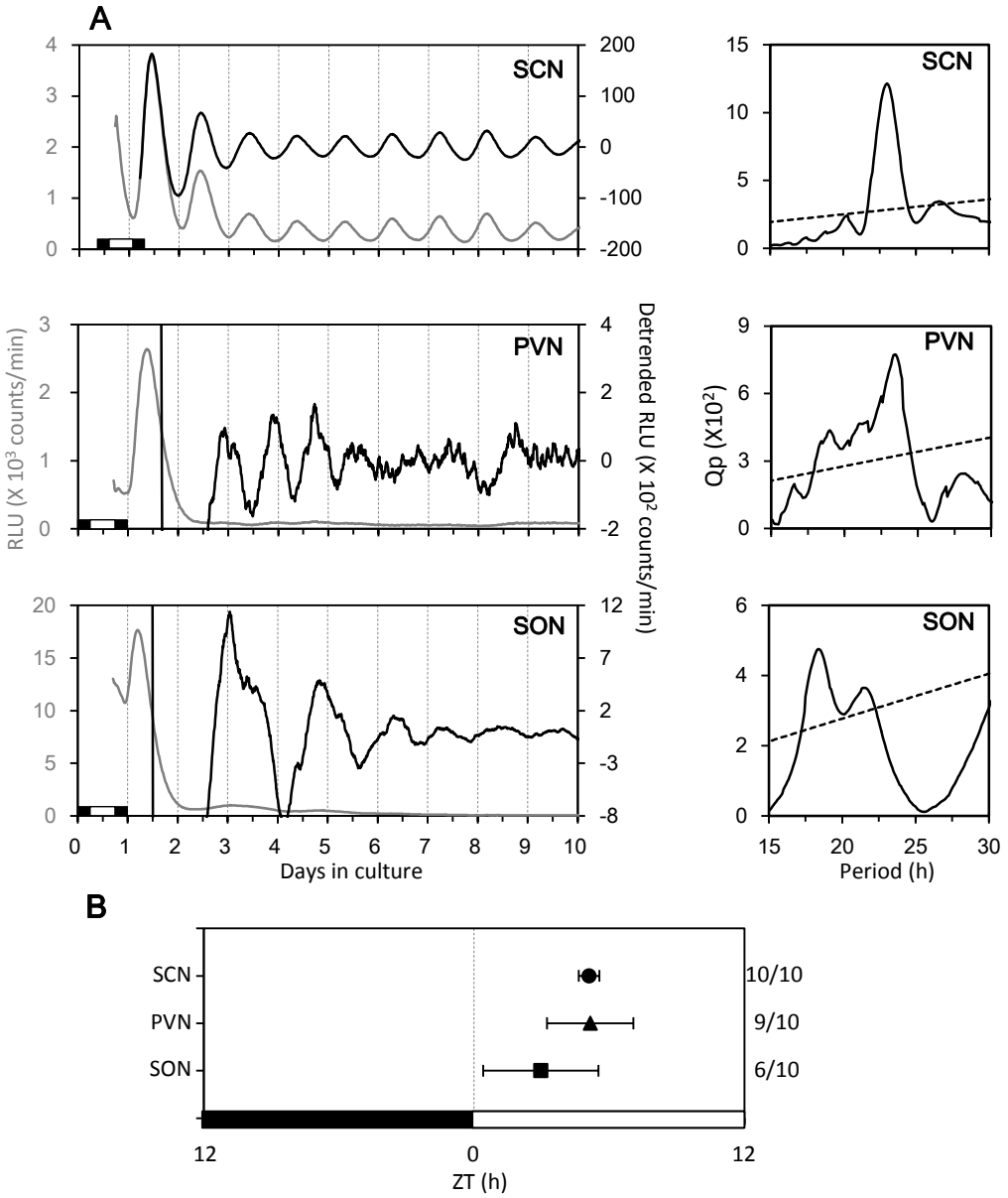
A
SCN
PVN
SON
RLU (X 10³ counts/min)
Detrended RLU (X 10² counts/min)
Days in culture
Qp (X10²)
Period (h)
B
SCN
PVN
SON
10/10
9/10
6/10
12
0
12
ZT (h)

Fig. 4

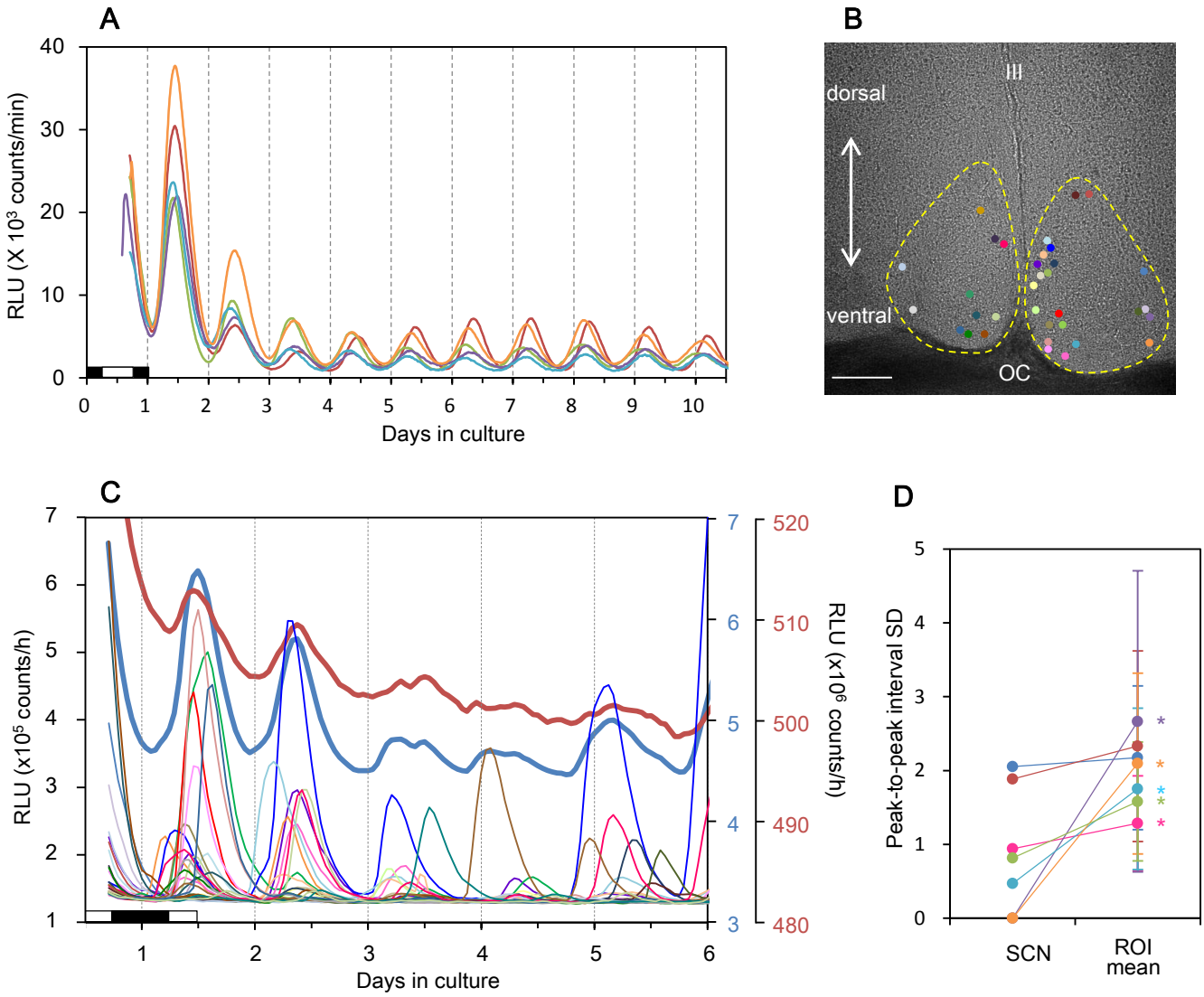
A
RLU (X 10³ counts/min)
Days in culture
B
III
dorsal
ventral
OC
C
RLU (x10⁵ counts/h)
RLU (x10⁶ counts/h)
Days in culture
D
Peak-to-peak interval SD
SCN
ROI mean

Fig. 5

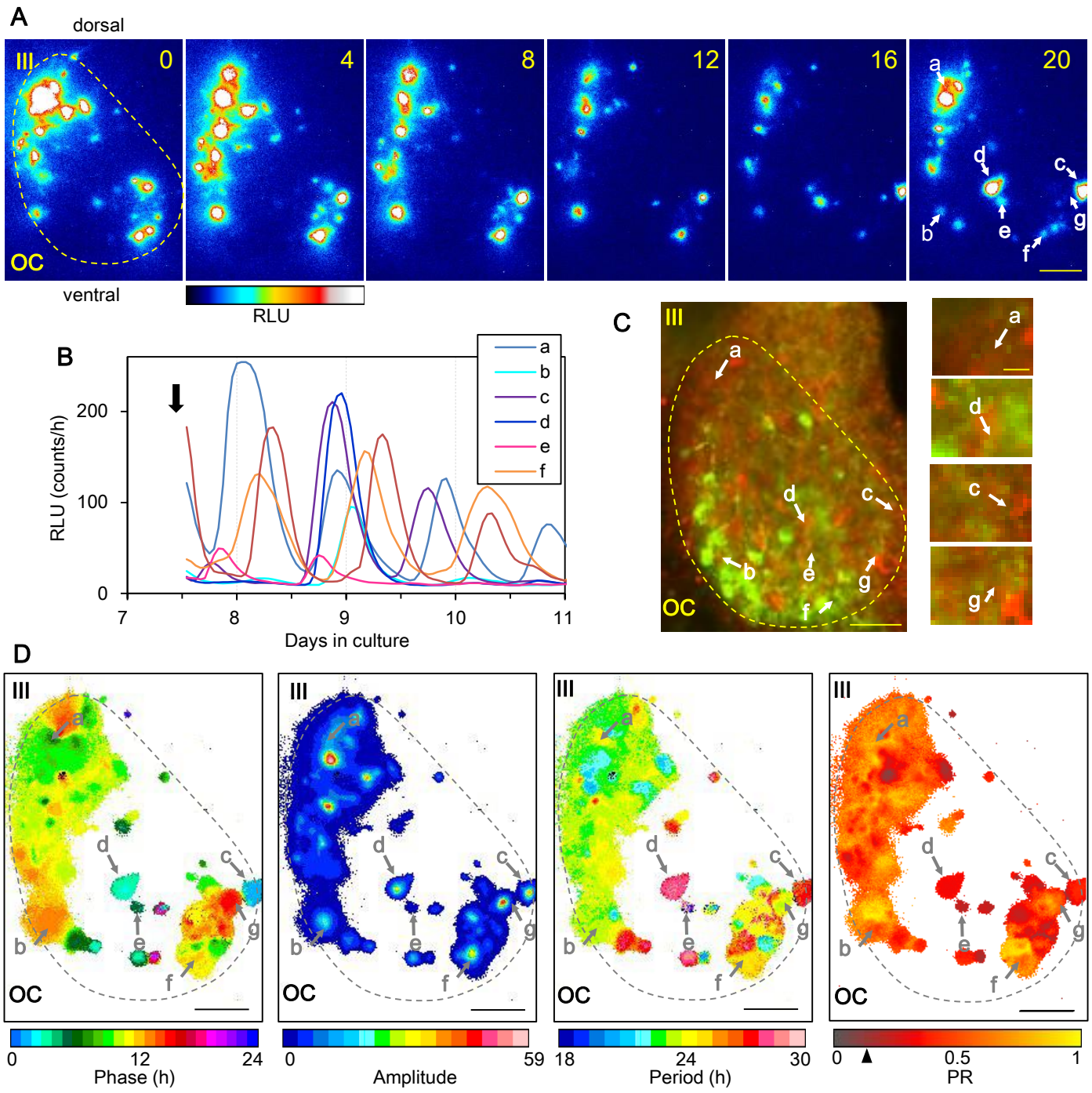
A
dorsal
III
0
4
8
12
16
20
a
b
c
d
e
f
g
OC
ventral
RLU
B
RLU (counts/h)
200
100
0
7
8
9
10
11
Days in culture
a
b
c
d
e
f
C
III
OC
D
III
OC
Phase (h)
0
12
24
Amplitude
0
59
Period (h)
18
24
30
PR
0
0.5
1

Fig. 6

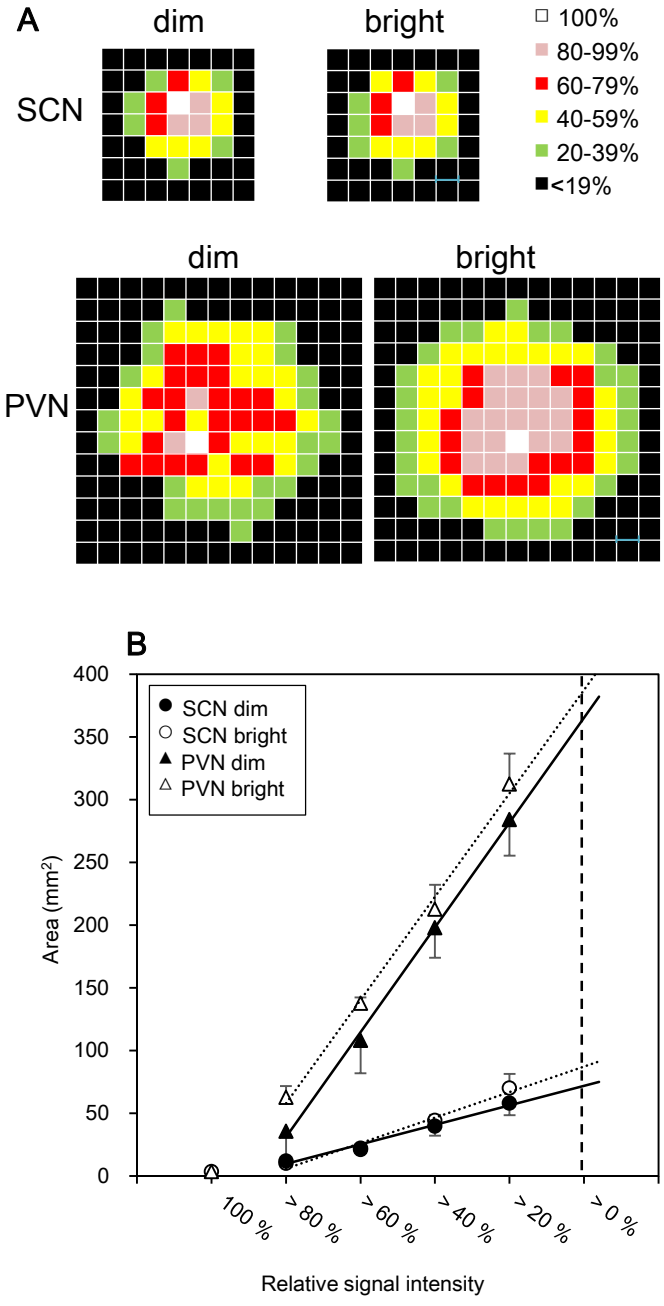
A
dim
bright
SCN
100%
80-99%
60-79%
40-59%
20-39%
<19%
dim
bright
PVN
B
SCN dim
SCN bright
PVN dim
PVN bright
Area (mm²)
400
350
300
250
200
150
100
50
0
100 %
> 80 %
> 60 %
> 40 %
> 20 %
> 0 %
Relative signal intensity